DOI: 10.21062/mft.2024.082 http://www.journalmt.com

Possibility of Eliminating Iron in Aluminium Alloy Through Sedimentation

Štefan Michna (0000-0001-5893-5050), Anna Knaislová (0000-0002-3508-9725)*, Jaroslava Svobodová (0000-0003-2175-1391), Jan Novotný (0000-0002-5784-6942), Lenka Michnová (0000-0003-0191-4632)
Faculty of Mechanical Engineering, J. E. Purkyne University in Usti nad Labem. Pasteurova 3334/7, 400 01 Usti nad Labem. Czech Republic. E-mail: stefan.michna@ujep.cz, anna.knaislova@ujep.cz, jaroslava.svobodova@ujep.cz, jan.novotny@ujep.cz, lenka.michnova@ujep.cz
*corresponding author

The article is dedicated to research on the elimination of high iron content (above 3-4%) in aluminium alloys through sedimentation. The aim was to determine the effect of sedimentation time on reducing the iron content in material from a refining bath with high iron content and to identify the phases formed in the structure. Melts were prepared from the material obtained from the refining bath, which consisted of an AlSi12 alloy with 3-4% Fe content. After melting, sedimentation was carried out for 2 hours, 4 hours, and 6 hours. Sedimentation was conducted while maintaining the alloy in a liquid state throughout the entire sedimentation period. After sedimentation and cooling of the castings, samples were taken to prepare metallographic specimens, and analyses were conducted to measure the iron content in the individual samples and to observe the reduction of iron content depending on the sedimentation time. Additionally, the identification and description of the intermetallic phases formed in the structures of the sedimenting castings from the refining bath were carried out using a scanning electron microscope with EDS analysis.

Keywords: AlSi12MgCuNi alloy, AlSi12Fe4 alloy, Alfination bath, Microstructure, Intermetallic phases

1 Introduction

Iron is always found in aluminium its alloys. It enters the melt in various ways, from the primary production of aluminium, through the dissolution of iron or from steel tools used in aluminium during the melting and casting process, as an impurity and contamination of secondary raw materials, in refining baths during the casting of automotive pistons, to intentional alloying with iron. Thus, iron is most commonly present in aluminium alloys as an impurity element but also as an alloying element in several alloys (e.g., EN AW 4006 – AlSi1Fe, EN AW 2031 – AlCu2.5NiMg, etc.). As an alloying element, iron improves the strength properties of aluminium alloys at higher temperatures and increases their hardness but decreases the ductility of the material. Partially, iron also improves the machinability of aluminium alloys. However, iron reduces corrosion resistance and can cause pitting corrosion; it also decreases the thermal and electrical conductivity of aluminium alloys and, due to the precipitation of brittle intermetallic phases, reduces fatigue properties and plasticity of the material. Therefore, iron forms intermetallic phases in aluminium alloys, given its low solubility in the solid state (approximately 0.03%). Iron forms intermetallic phases with aluminium, where the structure and type of crystal lattice of the resulting intermetallic phase differ from the original structure of the base metal, such as $FeAl_6$, $FeAl_3$, Fe_2SiAl_8, and $FeSiAl_5$. These intermetallic phases mainly negatively affect the mechanical properties of aluminium alloys. In Al-Cu alloys, iron forms the intermetallic phase Al_7FeCu_2, which depletes the solid solution of copper, thereby reducing the strength properties of Al-Cu alloys. Additionally, iron blocks grain growth when iron-rich dispersed particles are precipitated in the structure. Al_7FeCu_2 crystallizes in a tetragonal lattice with a density of 4.44 g/cm^3, while aluminium has a density of 2.702 g/cm^3 and crystallizes in a cubic K12 lattice. In Al-Cu-Ni alloys at elevated temperatures, iron increases strength properties. The intermetallic phase $FeAl_3$ crystallizes in a monoclinic lattice, with a density of 3.78 g/cm^3 and a relatively high melting point of 1160 °C. Its coarse crystals tend to crack and cause notches. These notches limit the formability and resistance to fatigue fractures in aluminium alloys [1-8].

The ternary phase diagram of Al-Si-Fe is quite complex and contains many phase transformations (Fig. 1). This system is characterized by a high number of ternary phases, stable and unstable. The presence of these phases influences mechanical properties, corrosion resistance, mechanical processing, etc. Currently, the phase diagram of the Al-Si-Fe system is not precisely established, and research is being conducted to supplement it for expansion and better understanding. Table 1 lists the structures that occur in the phase diagram of Al-Si-Fe [1, 2, 9, 10].

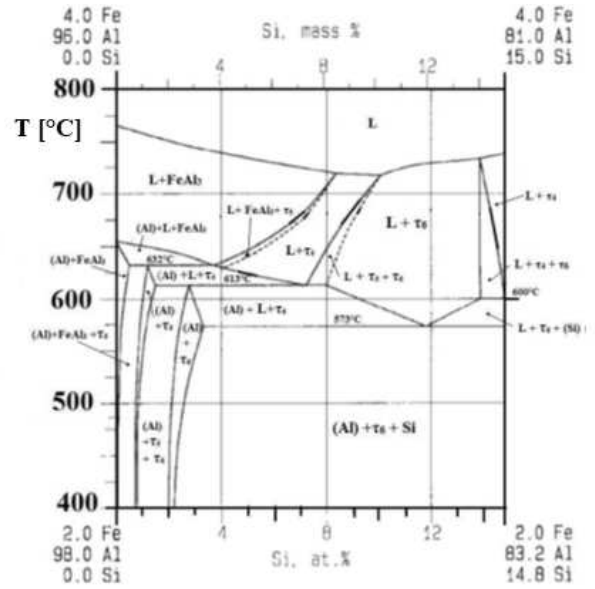

Fig. 1 *AlFe-Si phase diagram [1]*

The term "refining bath" refers to the melt of the aluminium alloy AlSi12, which is used in the technology of gravity casting aluminium pistons for internal combustion engines. Specifically, the refining bath is used to connect the cast iron ring carriers (lubricating and scraper rings on the piston) with the piston itself, which is made from the alloy $AlSi_{12}MgNiCu$ [11]. The $AlSi_{12}$ alloy (Table 2) has excellent casting properties, with good resistance to hot cracking, good machinability, weldability, high chemical resistance, and good corrosion resistance. This material is suitable for producing complex, thin-walled, and cyclically stressed castings. However, the material cannot be heat treated by precipitation hardening [12-15].

In the production of internal combustion engine pistons, cast iron ring carriers (Fig. 2) are immersed in the refining bath (melt of aluminium alloy AlSi12) and kept there for 3-4 minutes at a temperature of 720-730 °C. A layer from the refining bath forms over the entire surface of the ring carriers (Fig. 3). These treated carriers are then placed into a vertically divided metal mold. The mold is closed and filled with an aluminium alloy of similar chemical composition (AlSi12MgNiCu) to that of the refining bath, resulting in the casting of the piston and embedding of the cast iron carrier into the piston. Thanks to the aluminium layer on the cast iron carriers, the carrier bonds firmly with the aluminium material of the cast piston. After the casting solidifies, the mold is opened, and the piston casting proceeds to further technological processing (precipitation hardening, surface machining by turning), resulting in a finished piston.

Tab. 1 *Chemical notation of the structures τ5, τ6, τ4*

Structure	Chemical notation	Decomposition temperature [°C]
$\alpha = \tau_5$	$Al_{12}Fe_3Si_2$	855
	Al_8Fe_2Si	715
	$Al_{7,4}Fe_2Si$	710
$\beta = \tau_6$	Al_5FeSi	700
	$Al_{4,5}FeSi$	694
	$Al_9Fe_2Si_2$	667 ± 5
$\delta = \tau_4$	Al_4FeSi_2	865
	Al_3FeSi_2	834
	$Al_{2,7}FeSi_{2,3}$	-

Tab. 2 *Chemical composition of the $AlSi_{12}$ alloy [16]*

Element	Si	Fe	Cu	Mn	Mg	Cr	Ni	Zn	Pb	Sn	Ti
Element content [wt. %]	10.5-13.5	max. 0.40	max. 0.03	max. 0.35	-	-	-	max. 0.10	-	-	max. 0.15

When the iron content in the refining bath increases, it must be replaced, as it cannot be used for further refinement of the ring carriers. The threshold value for iron in the refining bath is a maximum of 4% Fe; if this value is exceeded, the refining bath must be replaced without fail. If the refining bath is not replaced and continues to be used with increased iron content, the embedding of the carriers into the piston will result in poor bonding of the carriers with the piston material. This will cause an increase in hardness of the surrounding material due to the presence of iron, leading to cracking of the material and destruction of the piston. This is because iron in aluminium and its alloys forms intermetallic phases, which tend to crack

(they are brittle).

Overall, a significant amount of refining bath with a high iron content of approximately 4% is generated as waste in the process of producing automotive pistons. This creates a major issue with its further utilization, with the main problem being the iron content. Thus, a method is being sought to effectively reduce the iron content in a significant portion of the material's volume and use it as secondary raw material in the production of aluminium alloys. The reason is not only to produce pistons of the required quality but also to increase cost-effectiveness and reduce costs due to the replacement of the refining bath. Therefore, a method is being sought to utilize as much refining bath as possible with sufficient purity [17].

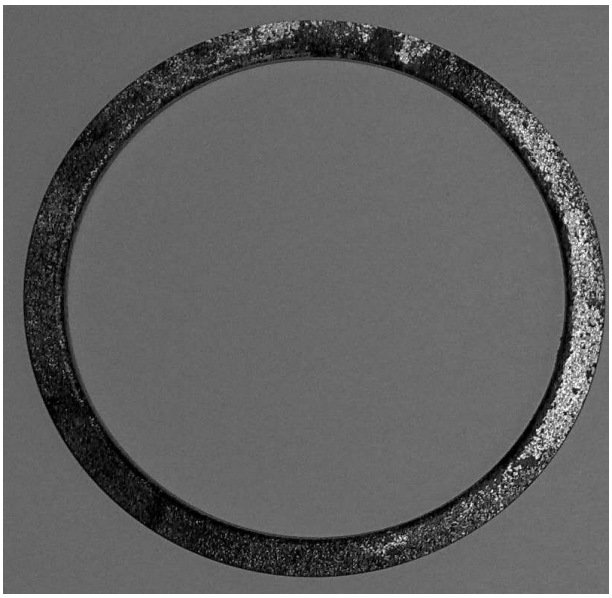

Fig. 2 *Cast iron carrier before immersion in the refining bath [17]*

Fig. 3 *Carrier with an aluminium layer formed [17]*

2 Experimental

A supply of discarded refining bath (alloy $AlSi_{12}Fe_4$) with a high iron content was secured, and a chemical analysis was performed using a portable spectrometer. The measurement results are shown in Table 3. From this material, samples for individual melts of the same weight were subsequently prepared and subjected to different sedimentation times after melting under the same conditions for the liquid metal. The material was melted in an electric resistance furnace at 780 °C, and after melting and removing dross from the surface of the melt, the melts were left in the furnace at 720 °C to sediment for 2, 4, and 6 hours. One melt was conducted without sedimentation, and all melts were performed in the same type and size of graphite crucible (Figs. 4, 5).

Tab. 3 *Chemical composition of refining bath*

Element	Si	Fe	Cu	Mn	Mg	Cr	Ni	Al
Element content [wt. %]	14.07 ± 1.5	3.60 ± 0.54	0.37 ± 0.04	-	-	-	0.72 ± 0.25	81.24 ± 3.05

Fig. 4 *Batch prepared for melting*

Fig. 5 *Melts after melting and sedimentation*

ISSN 1213–2489
e-ISSN 2787–9402

Fig. 6 *Casting of sedimenting refining bath*

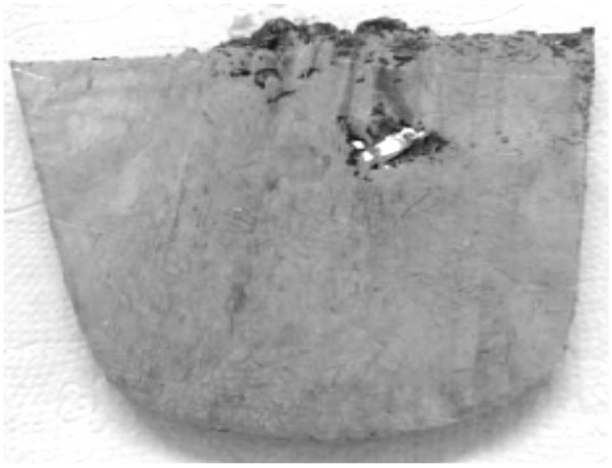

Fig. 7 *Sample from the casting of sedimenting refining bath after 2 hours*

After cooling, samples approximately 1.5 cm thick were taken from each casting, longitudinally from the center of the castings across their entire height (Figs. 6-9). Subsequently, the iron content in the samples was measured at specific distances from the bottom to the top of the castings using a portable spectrometer. The measured iron content values at specific points and in individual samples according to sedimentation time are shown in Table 4, which also includes the distances from the bottom of the casting. The results indicate that the effect of sedimentation on the elimination of Fe phases becomes apparent only in the 6-hour variant. In this 6-hour sedimentation, the highest concentration of iron is evident up to 4 cm from the bottom, i.e., within 1/3 of the total height of the casting.

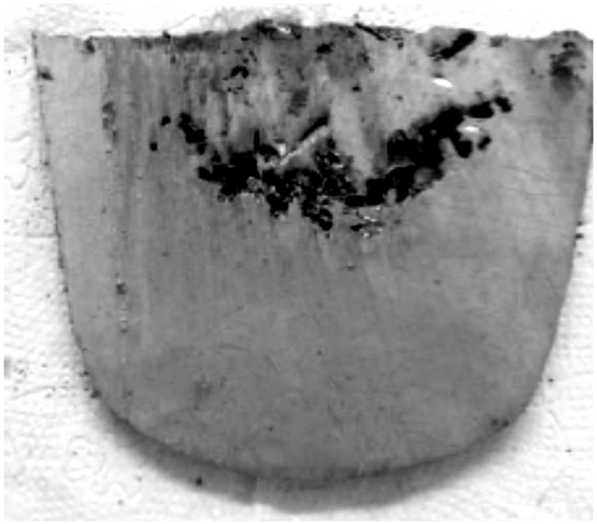

Fig. 8 *Sample from the casting of sedimenting refining bath after 4 hours*

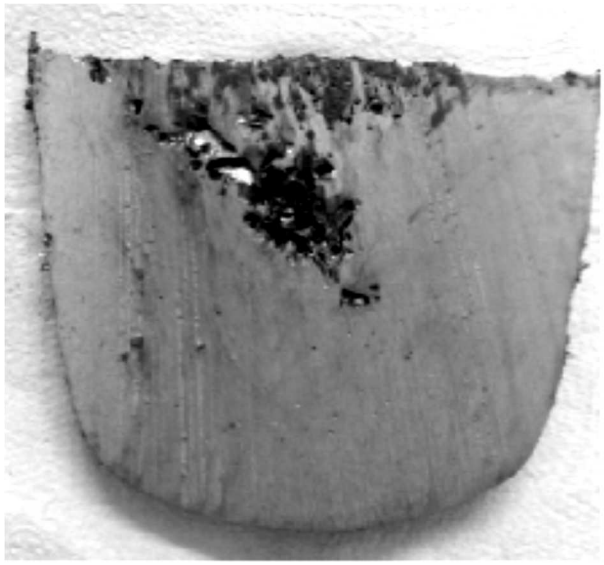

Fig. 9 *Sample from the casting of sedimenting refining bath after 6 hours*

Tab. 4 *Iron content depending on distance and sedimentation time*

Distance from the bottom of the casting [cm]	Iron content after sedimentation [%]		
	2h	4h	6h
0	4.41	3.41	4.12
2	2.92	3.55	9.63
4	5.22	4.02	5.28
6	2.57	3.23	2.40
8	1.54	4.18	2.86
10	2.95	2.56	2.22
12	3.92	3.29	3.60

indexed on http://www.webofscience.com and http://www.scopus.com

The next step involved taking and preparing metallographic samples to determine the phases formed in the casting structures. For preliminary phase identification, the Al-Fe-Si phase diagram was used, which allows to predict the expected phases based on the chemical composition of the supplied material. To identify and document the resulting structural phases, a confocal laser microscope and a scanning electron microscope were used to determine the chemical composition of the formed phases.

3 Results and discussion

For structural assessment and identification of individual structural components, a confocal laser microscope was used, mainly for the casting with 6 hours of sedimentation. From a chemical composition perspective, it practically represents an $AlSi_{12}Fe_4$ alloy. Identification of individual structural components in the $AlSi_{12}Fe_4$ alloy made it possible to identify the individual components of the structure, which were then subsequently analyzed using EDS on the scanning electron microscope. In Figure 10 and Figure 13, the microstructure of the $AlSi_{12}Fe_4$ alloy is documented, showing very coarse plate-like intermetallic phases, likely Al_5FeSi, and fine Si needles precipitated in the eutectic. Figure 11 shows plate-like intermetallic phases Al_5FeSi, Si needles, and light brown branched intermetallic phases, likely $Al_{12}(Fe,Mn,Cu)_3Si_2$ intermetallic phases with Cu content due to the brown or pink coloring and based on EDS analyses. Figure 12 documents a large cluster of light to brownish-colored branched intermetallic phases resembling "Chinese script," likely representing intermetallic phases of the $Al_{12}(Fe,Mn,Cu)_3Si_2$ or $Al_{12}(Mn,Cu)_3Si_2$ type based on coloration (presence of Cu), shape, and EDS analyses [18].

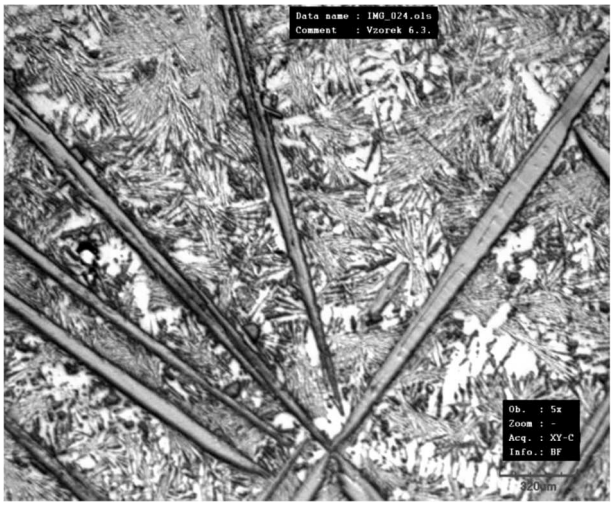

Fig. 10 *Coarse plate-like intermetallic phase and fine Si needles*

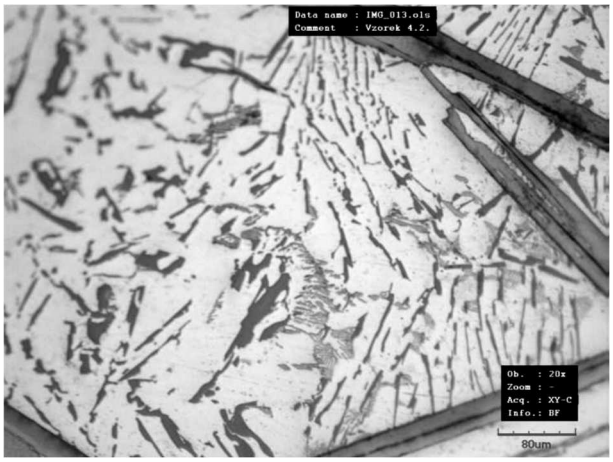

Fig. 11 *Coarse plate-like intermetallic phase (on the right), Si needles, and light brown branched intermetallic phases*

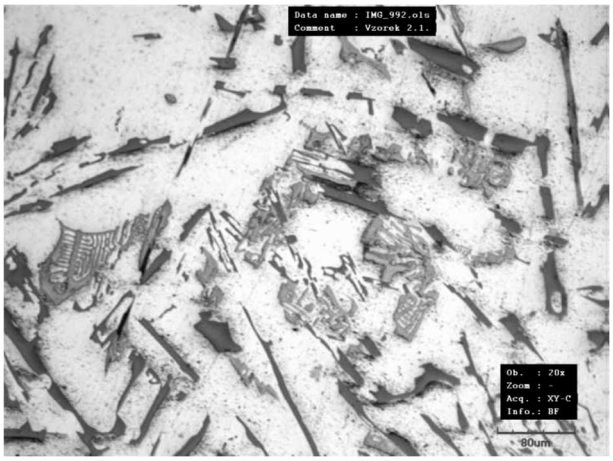

Fig. 12 *Large cluster of light to brown-colored branched intermetallic phases resembling "Chinese characters"*

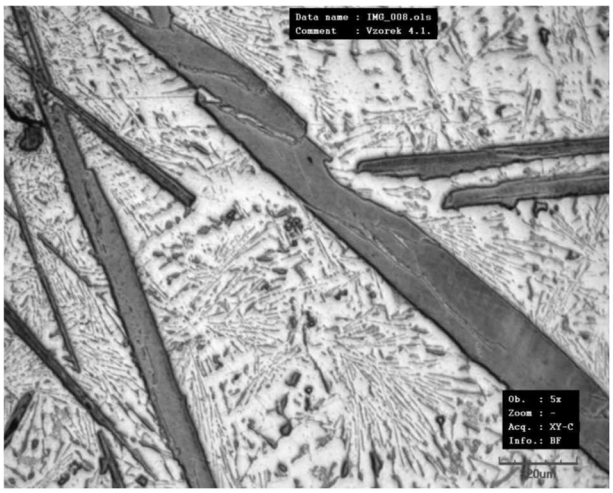

Fig. 13 *Coarse plate-like intermetallic phase and fine Si needles*

For chemical analysis of individual structural components in the AlSi12Fe4 alloy, a scanning electron microscope TESCAN VEGA 3 LMU equipped with a Bruker EDS analyzer was used. Point EDS analyses

of four different structural components were performed on the scanning electron microscope, including coarse irregular plate-like formations of various shapes and sizes up to several hundred micrometers, lighter coarser branching skeletal formations forming networks (so-called "Chinese characters"), irregular lighter needle-like branching skeletal formations, and large clusters of skeletal formations (appearing brown on the optical microscope) resembling "Chinese characters."

On Fig. 14, there are evident coarse irregular-shaped features of varying sizes up to several hundred micrometers, where the area EDS confirms the presence of aluminium 67.9 at. %, iron 17.29 at. %, and silicon 14.81 at. % (Fig. 15, Table 5). From the morphology of this structural component, EDS analyses, stoichiometric ratio within the chemical composition of the plate-like feature, and theoretical knowledge, it can be inferred that these are plate-like intermetallic phases of the Al_5FeSi type. Their overall occurrence in the structure is significant, as evident in the structure in Fig. 10 and Fig. 13. Especially, the intermetallic phase of the Al_5FeSi type, which occurs in large quantities in the structure of all castings subjected to sedimentation, is very dangerous because of its plate-like morphology, making it very brittle and prone to cracking. Its presence in the material will lead to the formation of cracks and the destruction of components due to the low plasticity of the material. Additionally, the corrosion properties of the material with the occurrence of the mentioned intermetallic phases with Fe will be poor.

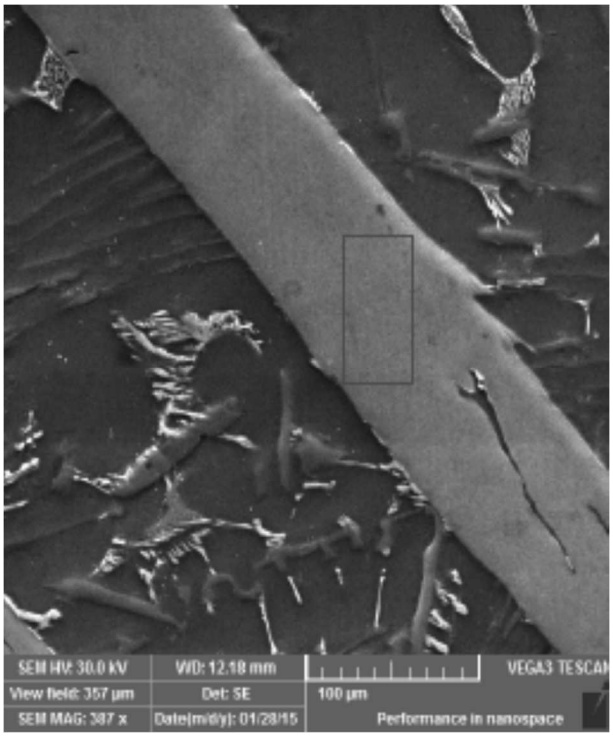

Fig. 14 *Selected area for area EDS analysis of the AlSi12Fe4 alloy*

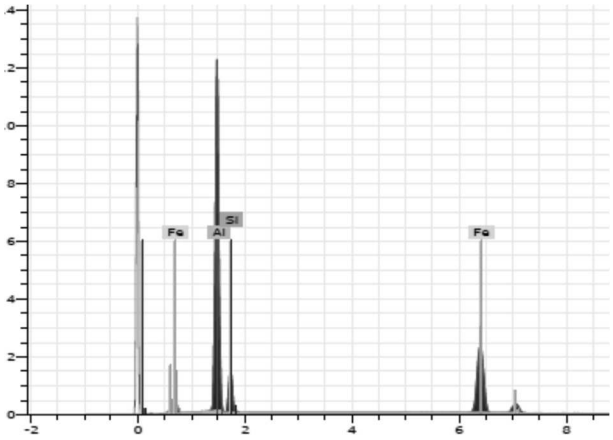

Fig. 15 *EDS analysis of individual elements*

Tab. 5 *Summary of the area analysis of the marked region in Fig. 14 with the concentration of individual elements in the AlSi12Fe4 alloy*

Spectrum:

Element	Series	unn. C [wt.%]	norm. C [wt.%]	Atom. C [at.%]	Error (3 Sigma) [wt.%]
Aluminium	K-series	51.94	57.01	67.90	8.00
Iron	K-series	27.37	30.04	17.29	2.31
Silicon	K-series	11.79	12.94	14.81	1.85
	Total:	91.09	100.00	100.00	

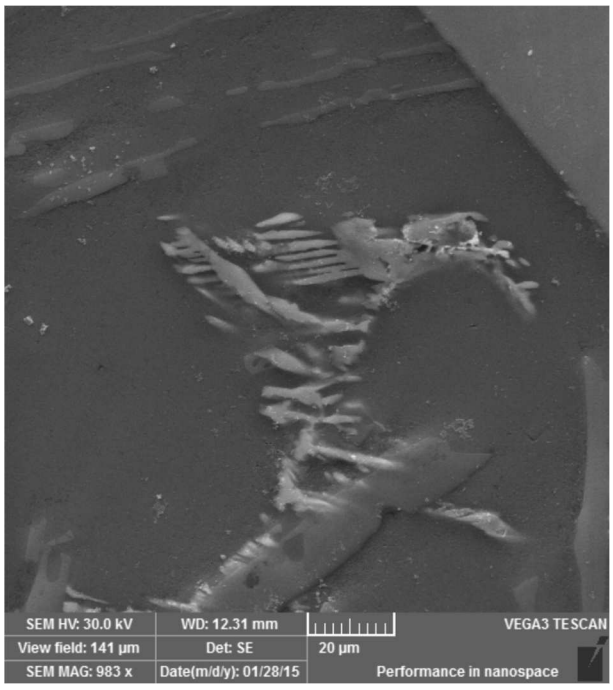

Fig. 16 *Selected area for area EDS analysis of the AlSi12Fe4 alloy*

Figure 16 shows brighter, coarser, branched skeletal structures forming irregular shapes and sizes, where area EDS confirms the presence of aluminium 82.12 at. %, iron 1.42 at. %, silicon 0.92 at. %, copper 2.93 at. %, and also a high content of nickel 12.58 at. % (Fig. 17, Table 6). From the morphology of this structural component, EDS analyses, stoichiometric ratios

within the chemical composition of the plate-like structure, and theoretical knowledge, it can be concluded that these are coarse branched complex intermetallic phases with the composition $Al_{58}Ni_9Cu_2FeSi$. The mentioned intermetallic phase has a very low content of silicon and iron but a high content of nickel. Its overall occurrence in the structure is very small and rare.

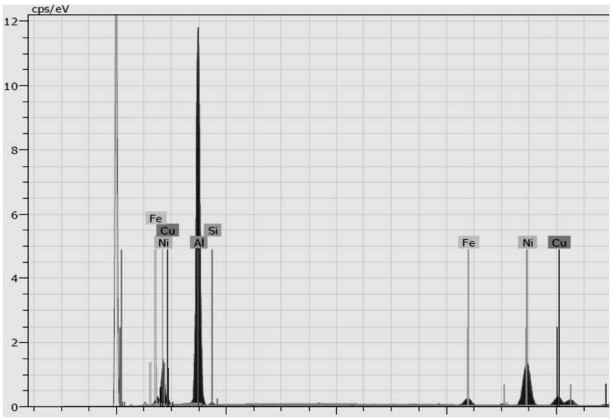

Fig. 17 *EDS analysis of individual elements*

Tab. 6 *Summary of the area analysis of the marked region in Fig. 16 with the concentration of individual elements in the AlSi12Fe4 alloy*

Spectrum:

Element	Series	unn. C [wt.%]	norm. C [wt.%]	Atom. C [at.%]	Error (3 Sigma) [wt.%]
Aluminium	K-series	57.44	68.25	82.12	8.82
Nickel	K-series	19.14	22.74	12.58	1.64
Copper	K-series	4.83	5.73	2.93	0.58
Iron	K-series	2.06	2.45	1.42	0.32
Silicon	K-series	0.69	0.82	0.95	0.27
	Total:	84.16	100.00	100.00	

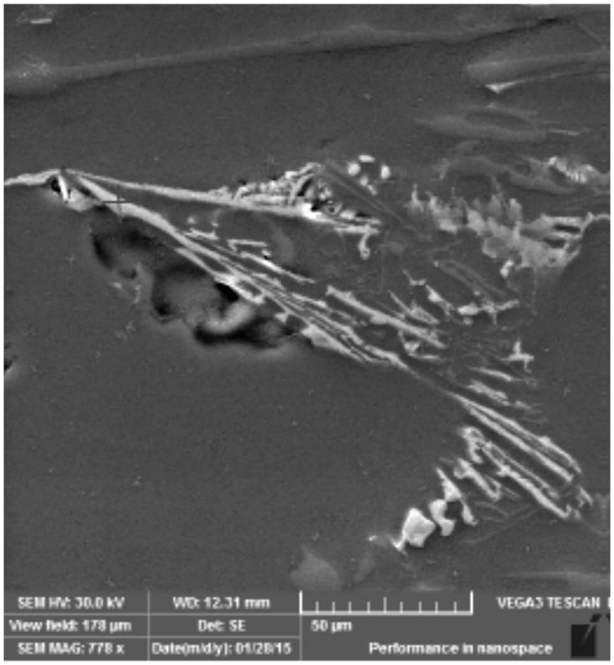

Fig. 18 *Selected area for area EDS analysis of the AlSi12Fe4 alloy*

On Fig. 18, irregular, brighter, needle-like branched skeletal structures forming a network of irregular shapes and sizes are visible, where area EDS confirms the presence of aluminium 76.46 at. %, iron 2.40 at. %, silicon 3.83 at. %, copper 2.96 at. %, and also a high content of nickel 15.77 at. % (Fig. 19, Table 7). From the morphology of this structural component, EDS analyses, stoichiometric ratios within the chemical composition, and theoretical knowledge, it can be concluded that these are needle-like branched complex intermetallic phases with the composition $Al_{49}Ni_{10}Fe_2Cu_2Si$. The mentioned intermetallic phase has a very low copper content but a high nickel content. Its overall occurrence in the structure is very small and rare.

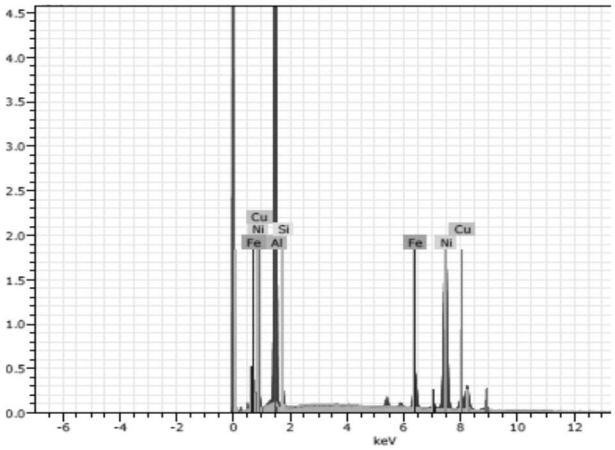

Fig. 19 *EDS analysis of individual elements*

Tab. 7 *Summary of the area analysis of the marked region in Fig. 16 with the concentration of individual elements in the AlSi12Fe4 alloy*

Spectrum: Acquisition 399

Element	Series	unn. C [wt.%]	norm. C [wt.%]	Atom. C [at.%]	Error (3 Sigma) [wt.%]
Aluminium	K-series	57.91	61.98	76.46	8.88
Nickel	K-series	25.98	27.81	15.77	2.13
Iron	K-series	3.76	4.02	2.40	0.45
Silicon	K-series	3.02	3.23	3.83	0.61
Copper	K-series	2.76	2.96	1.55	0.40
	Total:	93.43	100.00	100.00	

On Fig. 20, large rounded clusters of skeletal structures (appearing brown on the microscope) of the "Chinese characters" type, forming a network of irregular shapes and sizes, are visible, where area EDS confirms the presence of aluminium 79.04 at. %, iron 8.85 at. %, silicon 7.62 at. %, chromium 2.75 at. %, nickel 0.90 at. %, and manganese 0.83 at. % (Fig. 21, Table 8). From the morphology of this structural component, EDS analyses, stoichiometric ratios within the chemical composition, and theoretical knowledge, it can be concluded that these are needle-like branched complex intermetallic phases with the composition $Al_{29}Fe_3Si_3Cr$. Additionally, the mentioned intermetallic phase has a very low content of nickel and manganese.

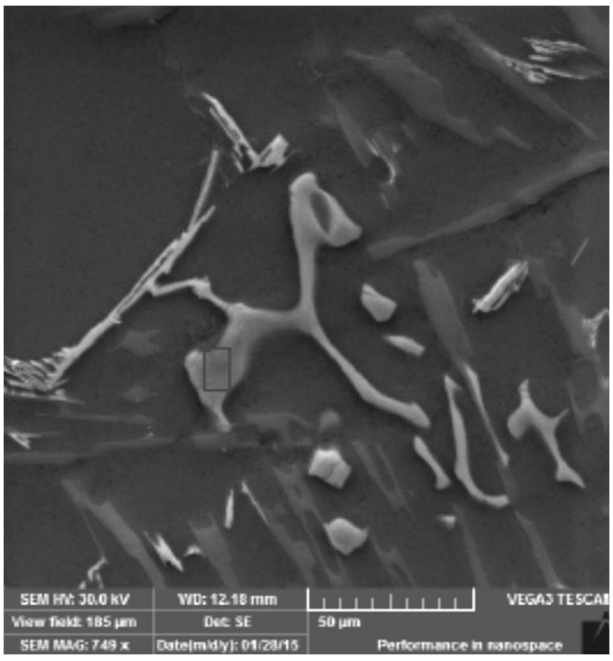

Fig. 20 *Selected area for area EDS analysis of the AlSi12Fe4 alloy*

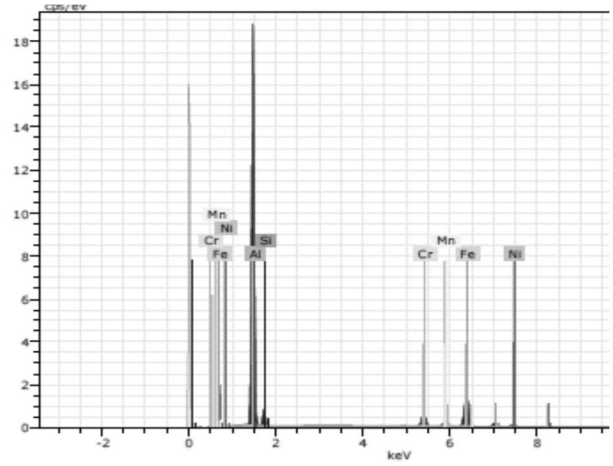

Fig. 21 *EDS analysis of individual elements*

Tab. 8 *Summary of the area analysis of the marked region in Fig. 16 with the concentration of individual elements in the AlSi12Fe4 alloy*

Spectrum:

Element	Series	unn. C [wt.%]	norm. C [wt.%]	Atom. C [at.%]	Error (3 Sigma) [wt.%]
Aluminium	K-series	63.16	69.18	79.04	9.61
Iron	K-series	14.63	16.03	8.85	1.26
Silicon	K-series	6.34	6.94	7.62	1.02
Chromium	K-series	4.24	4.64	2.75	0.46
Nickel	K-series	1.57	1.72	0.90	0.26
Manganese	K-series	1.35	1.48	0.83	0.23
	Total:	91.30	100.00	100.00	

4 Conclusion

The measured values of iron content in the AlSi12Fe alloy during sedimentation (2h, 4h, 6h) indicate that sedimentation for 2 and 4 hours does not lead to detectable sedimentation of iron intermetallic phases. From the results of sedimentation for 6 hours, it is evident that sedimentation to eliminate Fe phases occurs, with the highest concentration of iron occurring up to 4 cm from the bottom, i.e., up to 1/3 of the total height of the casting, ranging from 4.12 to 9.63 wt. % Fe. In the range of 6 – 12 cm from the bottom of the casting, the concentration of iron ranges from 2.22 to 3.60 wt. %.

Practically, in terms of chemical composition, it is an AlSi12Fe4 alloy with a lower content of chromium, nickel, and copper as accompanying elements originating from the dissolution of cast iron rings or the alloy itself. It was identified:

- Coarse irregularly shaped skeletal structures - coarse intermetallic phases of the Al5FeSi type - up to several hundred micrometers in size, following Si needles.
- Brighter, coarser branched skeletal structures - branched complex intermetallic phases with the composition $Al_{58}Ni_9Cu_2FeSi$ - forming a network of irregular shapes and sizes. These intermetallic phases have a very low silicon and iron content but a high nickel content.
- Irregular brighter needle-like branched skeletal structures $Al_{49}Ni_{10}Fe_2Cu_2Si$ forming a network of irregular shapes and sizes. These intermetallic phases have a very low copper content but a high nickel content.
- Large rounded clusters of skeletal structures of the "Chinese script" type forming a network of irregular shapes and sizes- needle-like branched complex intermetallic phases with the composition $Al_{29}Fe_3Si_3Cr$ with a very low nickel and manganese content.

Acknowledgement

Supported by the OP VVV Project Development of new nano and micro coatings on the surface of select-ed metallic materials - NANOTECH ITI II., Reg. No CZ.02.1.01/0.0/0.0/18_069/0010045.

EUROPEAN UNION
European Structural and Investment Funds
Operational Programme Research, Development and Education

MINISTRY OF EDUCATION, YOUTH AND SPORTS

References

[1] OSAWA, Y., TAKAMORI, S., KIMURA, T., MINAGAWA, K., KAKISAWA, H. (2007). Morphology of Intermetallic Compounds in Al-Si-Fe Alloy and Its Control by Ultrasonic Vibration. In: *MATERIALS TRANSACTIONS*, Vol. 48, No. 9, pp. 2467-2475.

[2] MICHNA, S. (2005). *Encyklopedie hliníku*. Adin, Presov

[3] MICHNA, S., NÁPRSTKOVÁ, N. (2012). *Tváření*, pp. 223. Jan Evangelista Purkyně University, Ústí nad Labem

[4] ŠERÁK, J., VOJTĚCH, D., NOVÁK, P., DÁM, K. (2011). *Využití sedimentační metody pro snížení obsahu železa v recyklovaných hliníkových slitinách.*

[5] HREN, I., MICHNA, S., DROZDYK, L., CAIS, J., MICHNOVÁ, L., SVOBODOVÁ, J., HODINÁŘ, L. (2018). Research of the Influence on the Modification of Beryllium in Al–Si Alloy. In: *Metallofizika i Noveishie Tekhnologii*, Vol. 40, No. 12, pp. 1637—1647.

[6] MICHNA, S., HREN, I., NOVOTNÝ, J., MICHNOVÁ, L., ŠVORČÍK, V. (2021). Comprehensive Research and Analysis of a Coated Machining Tool with a New TiAlN Composite Microlayer Using Magnetron Sputtering. In: *Materials*, Vol. 14, No. 13, pp. 3633.

[7] PRAKASH, U., RAGHU, T., KAMAT, S. V., GOKHALE, A. A. (1998). The effect of Mg addition on microstructure and tensile and stress rupture properties of a P/M Al-Fe-Ce alloy. In: *Scripta Materialia*, Vol. 39, No. 7, pp. 867-872.

[8] ZYSKA, A., BOROŃ, K. (2021). Comparison of the Porosity of Aluminum Alloys Castings Produced by Squeeze Casting. In: *Manufacturing Technology*, Vol. 21, No. 5, pp. 725-734.

[9] ATABAKI, M. M., NIKODINOVSKI, M., CHENIER, P., MA, J., HAROONI, M., KOVACEVIC, R. (2014). Welding of Aluminum Alloys to Steels: An Overview. In: *J. Manuf. Sci. Prod.* Vol. 14, No. 2, pp. 59-78.

[10] GHOSH, G., MATERIALS SCIENCE INTERNATIONAL TEAM, M., Al-Fe-Si Ternary Phase Diagram Evaluation - Phase diagrams, crystallographic and thermodynamic data: Datasheet from MSI Eureka in SpringerMaterials (https://materials.springer.com/msi/docs/sm_msi_r_10_014596_04), G. Effenberg, Editor., *MSI Materials Science International Services GmbH*.

[11] KAISER, M. S., SABBIR, S. H., KABIR, M. S., SOUMMO, M. R., NUR, M. A. (2018). Study of Mechanical and Wear Behaviour of Hyper-Eutectic Al-Si Automotive Alloy Through Fe, Ni and Cr Addition. In: *Materials Research*, Vol. No.

[12] MICHNA, S., MAJRICH, P. (2012). Possible ways of obtaining an aluminium alloy by non-traditional waste processing of aluminium beverage containers, In: *Manufacturing Technology*, Vol. 12, No. 2, pp. 169-174.

[13] MICHNA, S., MAJRICH, P. (2010). Vady u odlévaných automobilových pístů gravitačním litím do kovové formy. In: *Hutnické listy*, Vol. 1, No.

[14] TIWARI, V., PERIASWAMY, S. (2023). Compatibility of structural materials with AlSi12 alloys-based phase change material and increasing the corrosion resistance by ceramic coatings. In: *Journal of Energy Storage*, Vol. 72, No. 108526.

[15] MIKOLAJČÍK, M., TILLOVÁ, E., KUCHARIKOVÁ, L., PASTIEROVIČOVÁ, L., CHALUPOVÁ, M., UHRÍČIK, M., ŠURDOVÁ, Z. (2022). Effect of Higher Iron Content and Manganese Addition on the Corrosion Re-sistance of AlSi7Mg0.6 Secondary Alloy. In: *Manufacturing Technology*, Vol. 22, No. 4, pp. 436-443.

[16] http://www.trimet.cz/cz/sv_EN_AB-44200.php. 2024 [cited 2024 20.5.2024].

[17] MAJRICH, P., *Problematika propojování Fe a Al materiálu při odlévání pístů spalovacích motorů,* in Fakulta výrobních technologií a managementu. 2014, Jan Evangelista Purkyně University: Ústí nad Labem.

[18] GHOLIZADEH, R., SHABESTARI, S. G. (2011). Investigation of the Effects of Ni, Fe, and Mn on the Formation of Complex Intermetallic Compounds in Al-Si-Cu-Mg-Ni Alloys. In: *Metallurgical Materials Transactions A*, Vol. 42, No. 3447-3458.